Mahadik, Y., Robson Brown, K. A., & Hallett, SR. (2010). Characterisation of 3D woven composite internal architecture and effect of compaction. *Composites Part A: Applied Science and Manufacturing*, *41*(7), 872-880. https://doi.org/10.1016/j.compositesa.2010.02.019

CHARACTERISATION OF 3D WOVEN COMPOSITE INTERNAL ARCHITECTURE AND EFFECT OF COMPACTION

Y. Mahadik, K.A. Robson Brown and S.R. Hallett

Advanced Composites Centre for Innovation and Science, University of Bristol, University Walk, Bristol, BS8 1TR.

ABSTRACT

Yarn waviness and resin rich regions play a major role in 3D woven composite mechanical properties and failure. A detailed study of two angle-interlock 3D woven carbon fabrics has been carried out to characterise these architectural features and how they change under increasing levels of compaction. Computerised tomography (CT) x-ray scanning was used to capture the internal architecture of the fabrics. The study focussed on the out-of-plane crimp of the yarns and the size and shape of resin rich regions in consolidated panels. Results showed areas of high local crimp at weft/weaver interlace points. This was exacerbated at low levels of compaction but was eventually lowered under higher compaction levels. The appearance of resin channels was found to be heavily dependent on weave style, with large resin pockets appearing in weaver yarn planes which decreased significantly in size under compaction with distinctive changes in profile.

Keywords: A. 3-Dimensional reinforcement; A. Fabrics/Textiles; D. Radiography; E. Weaving

INTRODUCTION

3D woven carbon fibre fabrics consist of layers of warp and weft tows interlaced in the through-thickness direction by weaver yarns. This type of preform has an advantage over more commonplace unidirectional laminates and 2D woven reinforcements as it provides genuine through-thickness reinforcement, improving the interlaminar and damage tolerance properties of a composite.

3D woven fabrics exhibit a complex internal structure of interlaced tows which are deformed and distorted when woven and also when undergoing compaction in the moulding of the final composite. The detailed internal architecture of the fabric yarns plays a large part in determining the mechanical properties and failure mechanisms of a 3D woven composite.

Studies by Cox et al. [1,2] showed that out-of plane yarn crimp, caused by yarn nesting, played a large role in the tensile failure properties of a 3D woven composite and caused a drop in elastic modulus in both the warp and weft yarn directions. The study also highlighted the increased level of crimp in the weft yarn compared to the warp stuffers due to these yarns not being held under tension in the weaving process.

Similar findings were presented by Tan et al. [3] and Callus et al. [4]. The latter study presented results that showed the effect of resin channels on failure initiation and crack propagation. Resin rich regions present between yarns allowed cracks to propagate quickly and caused yarn failure at specific locations in the fabric architecture.

A number of studies have shown the large variations in mechanical properties produced by different interlock weave styles. Leong et al. [5] demonstrated how improvements could be made to yarn crimp and the presence of resin pockets by altering the path of weaver yarns specifically, leading to an improvement in strength and stiffness.

Although there has been some characterisation of 3D woven fabric architecture that considers yarn crimp and the spacing of the yarns (Lomov et al.[6]) and some work on modelling yarn deformations (Zhou et al.[7]), there is a distinct lack of detailed publications on experimental characterisation of out-of-plane crimp and resin pockets in 3D woven fabrics, and in particular the variation of these features under consolidation. This is in spite of the fact that previous literature highlights the crucial role they play in determining material properties.

There has however been some detailed analysis of 2D woven fabric architecture undergoing manufacturing processes. Statistical studies on yarn cross section shape in a 2D woven laminate under compaction (Saunders et al.[8]) and yarn crimp angles of nesting 2D woven layers (Yugartis [9]) demonstrated the feasibility of using cross section images and microscopy followed by detailed quantizing of tow shape to reflect the nature of internal fabric architectures. Similar studies by Chang et al.[10] and Chang et al [11] showed the measurement of yarn cross section shape and angle during draping, moulding and shearing of a 2D woven ply while Kim and Chang [12] related these changes in yarn geometry to variations in in-plane failure.

The above studies used a method of optical microscopy to provide images of yarn layers that were subsequently analysed. X-ray micro computed tomography (Micro-CT) is a more effective method of gathering internal images of structures. The Micro CT technique produces images of thin slices through the entire structure. This gives the user the ability to pinpoint areas of interest and also view them from any angle as well as providing a sequence of images that can be manipulated and analysed in image processing software. It has been shown to be effective in producing yarn cross section images of conventional 2D woven structures and 3D woven laminates (Summerscales et al. [13], Despentere et al. [14and Djukic [15]). Micro CT also allows the reconstruction of 3D images of composite features such as resin channels (Schell et al. [16]) and yarn paths (Schilling et al. [17] and Pandita [18]) from the 2D image slices.

This study presents a detailed analysis of yarn crimp and resin channel size and shape on two different 3D interlock fabrics using images obtained from micro CT scanning. In addition, it investigates the effect of increasing levels of compaction on the fabric architecture. This investigation was conducted with a view to subsequently linking the architectural features seen in the fabrics to failure mechanisms in a moulded 3D composite. The importance of yarn cross section shape as well as in-plane yarn waviness as architectural features is acknowledged but was beyond the scope of this study. It is suggested as a potential continuation of the work.

MANUFACTURE OF SAMPLES

Two fabrics, designated Fabric A and Fabric B, were each potted in the as-woven state and moulded to different thicknesses to cover a wide range of consolidated volume

fractions. The fibre volume fraction (VF) of consolidated samples was chosen to be in the range of 50% to 65% with four points evenly spaced in this range.

Fabric A is a layer-to-layer angle interlock fabric including seven layers of weft and six layers of warp yarns. One in three warp yarns is an interlacing weaver with the rest warp stuffers. Fabric B is a layer-to-layer angle fabric with alternating columns if weft of five and six layers producing a staggered weft pattern. The warp direction includes no stuffers, with every warp yarn being an interlacing yarn. Schematics of both fabrics are presented in Figure 1.

Figure 1 about here

To capture the as-woven fabric architecture, samples were potted in resin in small trays. The resin system chosen to consolidate the samples was SP115, a two-part epoxy resin/hardener system from Gurit Systems. It was chosen for its low viscosity at room temperatures and a clear finish when cured. Sections of fabric were placed in the trays and the resin poured on top. The trays were agitated using a small shaking table at a range of frequencies to dislodge air bubbles and help resin infusion.

A resin transfer moulding (RTM) infusion process was chosen to manufacture the 50%-65% VF samples. A two sided tool was designed so that it could produce samples of different volume fractions via the introduction of shims in the mould cavity (Figure 2). The shim plate consisted of a steel base plate of either 4mm or 5mm thickness with added layers of reinforced PTFE fabric. The 0.125mm thick PTFE fabric layers were

used to approach the target thickness for each sample more accurately. The resin system used was Prime 20 from Gurit Systems. It was chosen for its clear finish and range of cure cycles and hardeners. The infusion was conducted under 3 bar pressure and produced samples with good wet out and reliable thickness tolerances. There was no noticeable distortion of the samples from resin shrinkage or spring back that could have affected yarn geometries.

Figure 2 about here

SAMPLE SCANNING AND YARN IMAGE ACQUISITION

Small coupons suitable for x-ray computer tomography (CT) scanning were cut from the potted and RTM produced 90x150mm panels. The lengthwise direction of each coupon was aligned in the warp or weft direction to maximise the length of yarn captured in each specimen.

CT scanning apparatus from SkyScan was used to capture the internal architecture of the consolidated fabrics. A bespoke sample stage was designed and manufactured to house the samples and allow the x-ray source to approach the sample as closely as possible.

Despite trialling several different combinations of scanning parameters, the images produced exhibited quite poor contrast between yarns and resin as well as featuring a large amount of graininess which would hinder graphical characterisation of the architecture.

Image enhancement techniques were implemented in order to try and improve the quality of the images. It was found that using an intensity averaging technique across a number of slices cleared up the images significantly. This coupled with altering the brightness and contrast to capture the areas of interest produced satisfactory images.

RESULTS AND DISCUSSION: YARN CRIMP

Fabric A yarn crimp

The local, out of plane yarn crimp of individual tows was measured by discretizing a single tow using a series of points plotted along its centre line (Figure 3). The absolute local angle between two adjacent points could then be calculated from their coordinates (Figure 4). Yarn crimp was defined as the local angle of deviation from a specified horizontal datum for each yarn. The local yarn angle was measured along every yarn in 6-8 different slices in both the warp and weft directions. Local crimp data was recorded in the straight warp (Fabric A only), weft and weaver yarn planes for both Fabric A and Fabric B.

Figure 3 followed by Figure 4 about here.

Observations of CT scan slices of the as-woven Fabric A showed generally straight, low crimped warp yarns (Figure 5). The weft yarns are not held under tension in the weaving process, and therefore exhibited more crimp, especially at interlacing points with the weaver yarns. Weaver yarns showed the highest crimp as they are deliberately woven to interlace adjacent layers. Significant voids were present in all the samples (shown up as black in Figure 5) as the potting process used no pressure or injection to

improve resin infusion. They did not however influence the captured fabric architecture. The main aim was to set the fabric architecture in the as woven state without introducing unnecessary distortions.

Figure 5 about here.

These general features remained when the fabric was moulded to higher volume fractions. Figure 6 shows the mean yarn crimp in the weft, warp stuffer, and warp weaver yarns in Fabric A from the as-woven state to approximately 65% volume fraction. The mean yarn crimp is the average of every measurement of local angle across all the slices that were analysed. The error bars shown represent the standard deviation between crimp measurements for each yarn slice. The warp and weft were relatively straight in the as-woven state with only the weaver showing a high level of initial crimp due to the through-thickness weaving path.

Figure 6 about here.

At increasing levels of compaction the warp stuffer yarns remained relatively unaffected. Mean yarn crimp remained in the region of 2° with just a small rise at 50%-60% volume fraction. CT scan slices of a typical warp yarn layer at progressively higher volume fractions showed how the yarns retain their straightness. The warp yarns were not interlaced in the weaving process and subsequently had no inherently introduced deflection that could be exacerbated. Also, the yarns in the weft layers above and below

each warp yarn were evenly spaced and without large gaps. This architecture kept the warp yarns straight when the warp and weft yarns nested together under compaction.

The weft yarns in Fabric A exhibited more crimp in their as-woven state than the warp yarns. The mean weft crimp was 4° before compaction and with the yarns exhibiting local, high crimp areas at weft/warp weaver interlacing points.

The weft yarns showed an increase in overall mean crimp to 6° when compacted to 50% volume fraction and subsequently a decrease in crimp with increasing compaction. At 65% volume fraction the flattening effect of compaction reduced the crimp to approach the as-woven crimp level.

The changing architecture of the weft yarns that cause these statistical trends was clearly seen in CT scan images. At 50% volume fraction the major change from the as woven state was an increase in crimp due to the nesting of the yarns in the large inter-yarn gap left between the warp weaver and weft yarn at the interlacing point. This exacerbated the already introduced crimp at these locations (Figure 7).

The extra crimp in these locations spread out to parts of the yarn that lay between straight warp stuffers above and below. The gaps between the weft yarn and the straight warp stuffer sections were smaller than those found at the interlacing point allowing the weft to deflect less in these areas.

Figure 7 about here.

As the compaction increased to 60% VF, the inter yarn gaps gradually closed and the straightening effect of the compaction on the yarns grew. The smaller gaps between weft yarns and the straight warp yarns closed up first leading to a decrease in crimp in these regions. The even spacing of the warp yarns above and below the weft as well as the effect of tow spreading that further removed gaps in the warp layers lead to flatter surface when nesting with the weft yarn leading to lower crimp in the weft at these locations.

The larger inter-yarn gaps at weft/warp weaver interlace points, and therefore the highly crimped weft yarn regions at these locations, persisted up to 55%-60% VF but eventually flattened out at 65% VF as these larger gaps were closed (Figure 8).

Figure 8 about here.

These qualitative observations were borne out in the frequency distributions for local crimp in the weft yarns and provided a clearer picture of the distribution of crimp in the weft layers (Figure 9).

Figure 9 about here.

The initial increase in crimp at 50% volume fraction from the as-woven state was seen as a decrease in the proportion of 'straight' yarn (between 0-5° of crimp). The proportion of yarn crimped at 5° or less dropped from 67% to just over 50%. The increase of local areas of high crimp seen at the weft/warp weaver interlace points in the

x-ray slices was captured by the sharp increase in the proportion of yarn crimped by 15-20° from 2% in the as-woven state to 6%.

Further compaction to 55% and 60% volume fraction produced an increase in the proportion of straight yarn from 53% to 59%. However, the frequency distribution shows that the proportion of highly crimped yarn (15-20° and above) at 55-60% volume fraction remained constant. This can be explained by the flattening of the weft where it lay between areas of straight warp stuffers, away from the interlace points. Smaller inter-yarn gaps in these regions closed up at the lower volume fractions but the highly crimped regions at interlace points persisted due to the larger inter-yarn gaps.

At the highest level of compaction, at 65% volume fraction, the flattening effect reached the interlace points alongside a further increase in the flattening between straight warp areas. This was seen as an increase in the proportion of straight yarn along with a decrease in the proportion of highly crimped yarn in the crimp frequency distribution data.

Areas of high local crimp remain throughout the compaction range with 2% of the yarn seen exhibiting crimp of over 20°. This was attributed to the areas of weft at the surface interlacing points which remain in a highly crimped state throughout the compaction process. The weaver yarns were pushed down at the surface by the tool face, forcing the surface weft yarn to be deflected.

The Fabric A warp weaver yarns interlace the layer of weft above and below to provide through-thickness reinforcement. This leads to them being deliberately crimped in the weaving process in order to trace the desired path in the weave style. The mean local crimp for the warp weavers in the as woven state was 12° (refer back to Figure 6), much higher than the warp and the weft. The initial compaction to 50% volume fraction reduced this value to 8°. This was due to the large decrease in height of the fabric in the through thickness direction, counteracting the path of the weavers that traverse between weft layers.

Further compaction to 60% appeared to have little effect on the mean crimp, but a closer look at the architecture seen in the CT scan slices and from the frequency distribution provided a clearer picture of the more subtle changes in the crimp of the yarn (Figure 10).

Figure 10 about here.

The frequency distribution of local crimp angles showed a steady rise in the proportion of yarn at low crimp (0-5°) between 50% and 60% volume fraction. The proportion of 'straight' yarn rose from 33% to 48%. However, the amount yarn at higher crimp levels (15-30°) remained between 10-15% with the amount of crimp at 25-30° having showed a small increase.

These conflicting trends were thought to be the reason that the overall crimp stayed fairly constant between 50%-60% volume fraction.

At the higher levels of compaction up to 65% volume fraction, the flattening effect of yarn nesting increased and was sufficient to extend to the interlaced regions leading to a sharp drop in overall crimp to 6° and a decrease in the proportion of yarn showing crimp greater than 15°.

Fabric B yarn crimp

Fabric B was constructed using a different weave style that included no straight warp stuffers, with every warp yarn being a weaver that interlaced the next layer of weft yarns. The weave pattern also incorporated a staggered weft pattern that allowed the weft yarns to lie in between the weavers. The weft yarns subsequently exhibited less local deflection at interlace points giving rise to a very low crimp state in the weft direction in the as-woven fabric (Figure 11).

Under compaction, this initial low crimp in the weft was quickly lost. The mean crimp of the weft yarns rose from 2° in the as-woven state to 8° at 60% volume fraction. This was caused by the gaps between the weft and interlacing warp decreasing and introducing local deflections at interlacing points. Fabric B has a much higher occurrence of interlacing points due to every warp yarn being an interlacing yarn leading to a much greater presence of local regions of high crimp in these areas. The large increase in crimp in a more dispersed pattern was reflected by the high scatter in the data.

Figure 11 about here.

The mean crimp trends were reflected by the local crimp frequency distribution results. The proportion of ‘straight’ (0-5° crimp) weft yarn declined sharply from nearly 90% in the uncompressed state to under 40% at 60% volume fraction. In addition, the proportion of yarn that was considered to be highly crimped (15° and above) rose from 1% to approximately 14%.

As seen with the previous fabric, the amount of crimp seen in the weft yarns in Fabric B begins to diminish at 65% volume fraction. The mean crimp dropped from 8° at 60% volume fraction to just over 6.5° at 65% volume fraction. There was also an expected rise in the proportion of yarn crimped between 0-5° from 40% to 48% and a small drop in the proportion of highly crimped yarn, 15° and above, from 14% to 9%. This was due to the high degree of compaction flattening out the staggered weaver columns to allow the weft to lie in a straighter path.

These results are well illustrated by CT scan slices at 50% and 65% volume fraction with the slices showing the crimp being introduced at interlace points at 50% volume fraction and the flattening of the yarn at 65% volume fraction (Figure 12).

Figure 12 about here.

The Fabric B weaver yarns showed a large drop in crimp from 11.5° in the as-woven state to a roughly constant mean crimp level of 6.5-7° at volume fractions between 50% and 65%. As seen in the Fabric A, the flattening is caused by yarn nesting and the

closing up of the inter yarn gaps. Local regions of high crimp still occurred at various points on the weaver, especially at weft interlacing points where the inter yarn gaps are largest and least likely to be affected by the overall flattening of the fabric.

RESULTS AND DISCUSSION: RESIN POCKETS

Large and distinctive resin channels were seen to occur along the warp weaver yarns in the as woven state of both the fabrics. These were caused by the path of the yarn leaving large gaps between yarn layers where resin rich regions subsequently developed. Resin pockets seen in the weft yarn planes were orthogonal cross sections of the channels in the warp direction. The resin channel dimensions and volume discussed in this section refer to single one of these typical regions that occur in layers in the warp weaver yarn planes. Figure 13 shows a 3D representation of one of these channels and the images they produce when sectioned in the warp weaver and weft direction. The average dimensions of a single resin pocket were calculated from the yarn images by digitally separating the resin and yarn and outlining the resin rich regions. Resin pocket dimensions were measured in 6-8 slices in each yarn direction for each volume fraction. Results presented are the mean of all measured dimensions across the slices in a particular volume fraction sample.

Figure 13 about here.

Fabric A Resin Pockets

The compaction process progressively closed up the inter-yarn gaps, decreasing the size of the major resin pockets in the weaver direction dramatically. The volume of a typical warp weaver resin channel dropped from 10mm^3 in the as-woven state to 0.22mm^3 at 65% volume fraction.

A major trend in the measured dimensions of a resin pocket was a large decrease in resin pocket length with increasing compaction. The average length of each pocket dropped sharply from 6.1mm at 55% to 2.6mm at 60% volume fraction (Figure 14). This was due to weaver resin pocket retaining its distinctive shape, spanning one half of the repeating unit of the binder shape from the as-woven state up to 55% volume fraction but then closing up in the centre to form two distinct, shorter channels at further levels of compaction.

An expected drop in resin channel height due to the reduction in thickness of the fabric was also observed. The width of each channel was dependent on the width of the inter yarn gap left at the weaver/weft interlacing point and was less affected by the compaction of the fabric showing a smalldecrease from 1.4mm to 1mm.

Overall, the number of resin rich regions seen in each of the yarn directions (straight warp, weft and warp weaver) decreased sharply.

Figure 14 about here.

The above trends were confined to the internal resin channels away from the surfaces of the fabric. Surface resin channels are not bounded by yarns on one side and subsequently remain large. The surface channels retained the approximate size and shape seen at 50% volume fraction right up to 65%volume fraction.

Fabric B Resin Pockets

Fabric B also showed significant resin rich regions in the as woven state and throughout the volume fraction range. Internal resin pockets lay between warp weavers where the angle of the yarns let gaps remain (Figure 13). The Fabric B weave style used every warp yarn as an interlacing weaver and so these resin channels are much more prevalent than in Fabric A where two out of every three warp yarns were not interlaced and had negligible resin rich regions

The staggered weft patterns inherent in the Fabric B weave style allowed the weft yarns to nest between the warp weaver yarns and to break up the resin channels in the length direction giving a series of small diamond shaped resin pockets which had a much lower warp-weft aspect ratio than the resin regions of the Fabric A. In addition, the staggered pattern positioned the weft so that it touched the weaver yarns above and below. This led to fewer resin rich regions in a cross section through a weft yarn layer. However, a wide spacing was left between the weft layers and led to the resin channels to form between the weft yarns rather than underneath or over each yarn as in Fabric A. (Figure 15).

Figure 15 about here.

The resin pockets were on average significantly smaller (3mm^3) in the as woven state compared to the longer, uninterrupted channels in Fabric A (12mm^3). The total volume of each pocket declined sharply under the initial compaction of the fabric at 50% volume fraction to 0.5mm^3 and then saw a smaller decrease to 0.2mm^3 at 65% volume fraction.

Compaction of the fabric in the through-thickness direction largely affected the height of the resin channel but had relatively little effect on the width and length after the initial large drop in resin channel volume from the as-woven state. The height of the channel decreases from 1.8mm at 50% volume fraction state to 0.3mm at 65% volume fraction. The length shows a small reduction from 3 mm to 1 mm and the width of the resin pocket, determined by the weft yarn spacing, remained largely unchanged. See Figure 16 for detailed breakdown of resin pocket dimension.

Figure 16 about here.

As with Fabric A, the above analysis considers the internal resin channels away from the surface of the fabric. Much larger resin rich regions were present on the surface of the fabric where there was no further layer of weaver yarns above or below to close up the inter yarn gaps under compaction. These remained significantly greater in volume as well as having a greater length and height than the internal resin channels throughout the compaction range. They were less prevalent however, occurring only once per

binder repeating unit at a peak or a trough depending on which surface the resin pocket lay on.

CONCLUSIONS

A detailed, experimental characterisation of yarn crimp and resin pocket size and shape was conducted on two angle interlock fabrics.

The internal architecture of the fabrics was captured using an x-ray computer tomography (CT) scanning technique and the developed yarn images post-processed using a series of image analysis techniques. A wealth of data was produced and allowed reliable conclusions to be drawn from statistical analyses. CT scanning allowed the internal structure of the fabric to be viewed without the need for lengthy polishing and optical microscopy techniques. It also allowed easy manipulation of viewing angles and produced an image set that could be effectively digitised for analysis. Technical challenges included the limited sample size that could be scanned and the difficulty in producing good images due to the poor contrast between carbon fibre and epoxy resin.

Local, out of plane yarn crimp was recorded for each of the yarn directions in both fabrics over the volume fraction range. Non interlaced warp yarns, the warp stuffers present in Fabric A, were held in tension in the weaving process and show a low crimp in the off-the-loom fabric. This low crimped state remained up to 65% volume fraction.

Crimp in the weft yarns of Fabric A was dominated by the local architecture at weft/weaver interlacing points. The weaver yarns passed under or over a weft yarn at these points causing it to deflect, creating a local area of high crimp. This local high

crimp was exacerbated at lower volume fractions due to yarn nesting in the large inter yarn gap that accompanies the interlace point. Sections of the weft yarn away from the interlacing points flattened much more readily at lower volume fractions and exhibited lower crimp. At volume fractions close to 65%, the flattening effect of compaction reached the interlaced points and caused a sharp decrease in overall weft crimp.

Fabric B showed a very similar trend but incorporated a much higher proportion of weaver yarns, and therefore a greater number of weft interlacing points which caused the crimp in the weft yarns in this fabric to be higher when compacted. Fabric B demonstrated that the weave style can lower the initial as-woven weft crimp by staggering the weft pattern. This low crimp state did not survive the compaction process however.

A small proportion of the weft yarn in both fabrics remained highly crimped even at high levels of compaction. Local highly crimped areas were seen at surface interlace points throughout the fabric.

The weaver yarns in both fabrics showed the highest level of crimping in the off the loom state as they are deliberately deflected in order to interlace the adjacent layer of weft yarns. The compaction of the fabric flattened these yarns considerably but regions of high crimp remained especially at weft/weaver interlacing points.

Large resin pockets were present in both fabrics in both the as-woven state and throughout the compaction regime. The major resin channels existed between warp

weaver yarns. The resin pocket in Fabric A was much longer in the as woven state compared to Fabric B where the staggered weft pattern broke up the resin channels more effectively.

The internal resin channels away from the surface of the fabrics collapsed under compaction to one tenth of their as-woven size but remained a significant feature. The long internal resin pockets in Fabric A splits into distinct, smaller channels at 60% volume fraction and above. Both fabrics exhibited larger resin channels on the surface throughout the compaction range.

REFERENCES

[1] Cox BN, Dadkhah MS, Morris WL, Flintoff JG. Failure mechanisms of 3D woven composites in tension, compression, and bending. Acta Metallurgica et Materialia 1994; 42(12): 3967-3984.

[2] Cox BN, Dadkhah MS, Morris WL. On the tensile failure of 3D woven composites. Composites - Part A: Applied Science and Manufacturing 1996; 27(6): 447-458.

[3] Tan P, Tong L, Steven GP, Ishikawa T. Behaviour of 3D orthogonal woven CFRP composites. Part I. Experimental investigation. Composites - Part A: Applied Science and Manufacturing 2000; 31(3): 259-271.

[4] Callus PJ, Mouritz AP, Bannister MK, Leong KH. Tensile properties and failure mechanisms of 3D woven GRP composites Composites - Part A: Applied Science and Manufacturing 1999; 30(11):1277-1287.

[5] Leong KH, Lee B, Herzberg I, Bannister MK. Effect of binder path on the tensile properties and failure of multilayer woven CFRP composites, Composites Science and Technology 2000; 60 (1) :149-156.

[6] Lomov SV, Ivanov DS, Perie G, Verpoest I. Modelling 3D fabrics and 3D reinforced composites: challenges and solutions. Conference Proceedings:1st World Conference on 3D fabrics; Manchester 2008.

[7] Zhou G, Sun X, Wang Y, Multi-chain digital element analysis in textile mechanics. Composites Science and Technology 2004; 64:239–244.

[8] Saunders RA, Lekakou C, Bader MG. Compression and microstructure of fibre plain woven cloths in the processing of polymer composites. Composites Part A 1998; 29A: 443-454

[9] Yugartis SW, Morey K. Measurement of yarn shape and nesting in plain-weave composites. Composites Science and Technology 1993; 46:39-50.

[10] Chang SH, Sutcliffe MPF, Sharma SB. Microscopic investigation of tow geometry changes in a woven prepreg material during draping and consolidation. Composites Science and Technology 2004; 64:1701-1707.

[11] Chang SH, Sharma SB, Sutcliffe MPF. Microscopic investigation of tow geometry of a dry satin weave fabric during deformation. Composites Science and Technology 2003; 63: 99-111.

[12] Kim S., Chang .H. The relation between compressive strength of carbon/epoxy fabrics and micro-tow geometry with various bias angles. Composite Structures 2006; 75: 400-407.

[13] Summercales J, Russell PM, Lomov S, Verpoest I, Parnas RS. The fractal dimension of x-ray tomographic sections of a woven composite. Advanced Composite Letters 2004; 13(2): 133-121.

[14] Desplentere F, Lomov SV, Woerdeman DL, Verpoest I, Wevers M, Bogdanovich A. Micro-CT characterization of variability in 3D textile architecture. Composites Science and Technology2005; 65: 1920-1930.

[15] Djukic L. Tow visualistaion in woven composites using x-ray computed tomography. Recent Advances in Textile Composites2008; 417 -425

[16] Schell JSU, Renggli M, van Lenthe GH, Müller R, Ermanni P. Micro-computed tomography determination of glass fibre reinforced polymer meso-structure. Composites Science and Technology 2006; 66: 2016-2022.

[17] Schilling PJ, Bhanuprakash RK, Tatiparthi AK, Verges MA, Herrington PD. X-ray computed microtomography of internal damage in fiber reinforced polymer matrix composites. Composites Science and Technology 2005; 65: 2071-2078.

[18] Pandita SD, Verpoest I. Prediction of the tensile stiffness of weft knitted fabric composites based on x-ray tomography images. Composites Science and Technology 2003; 63: 311-325.

Fabric A

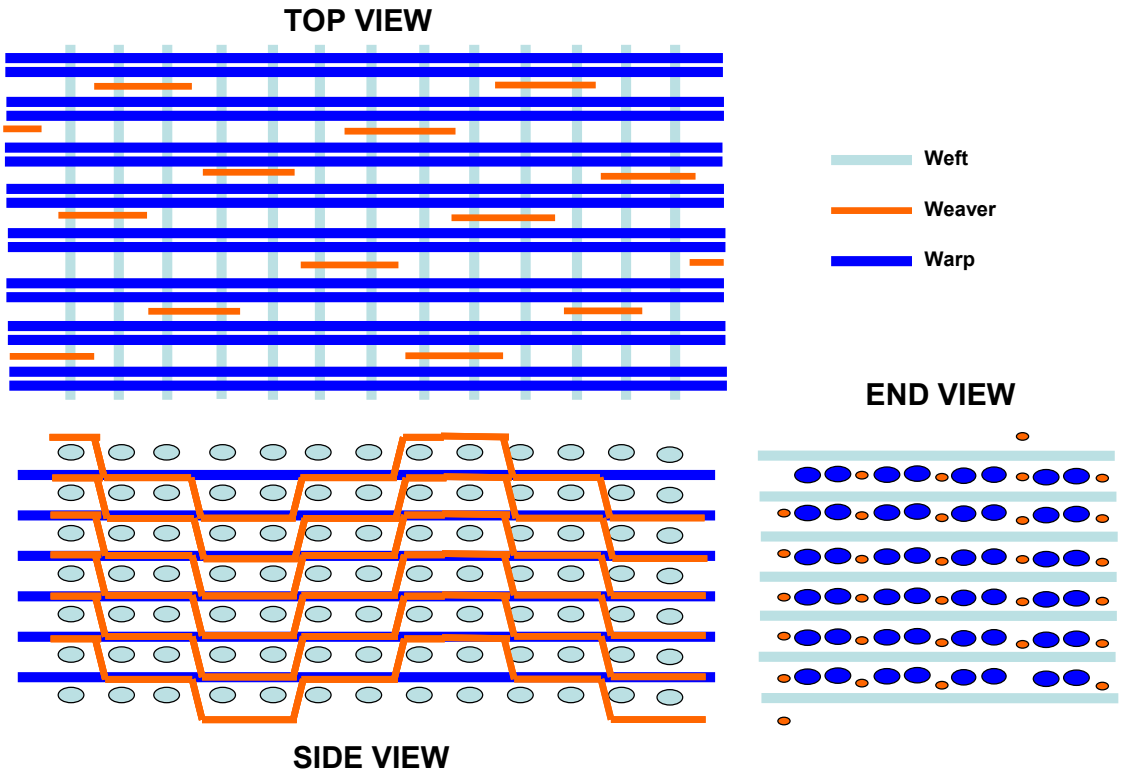

Fabric B

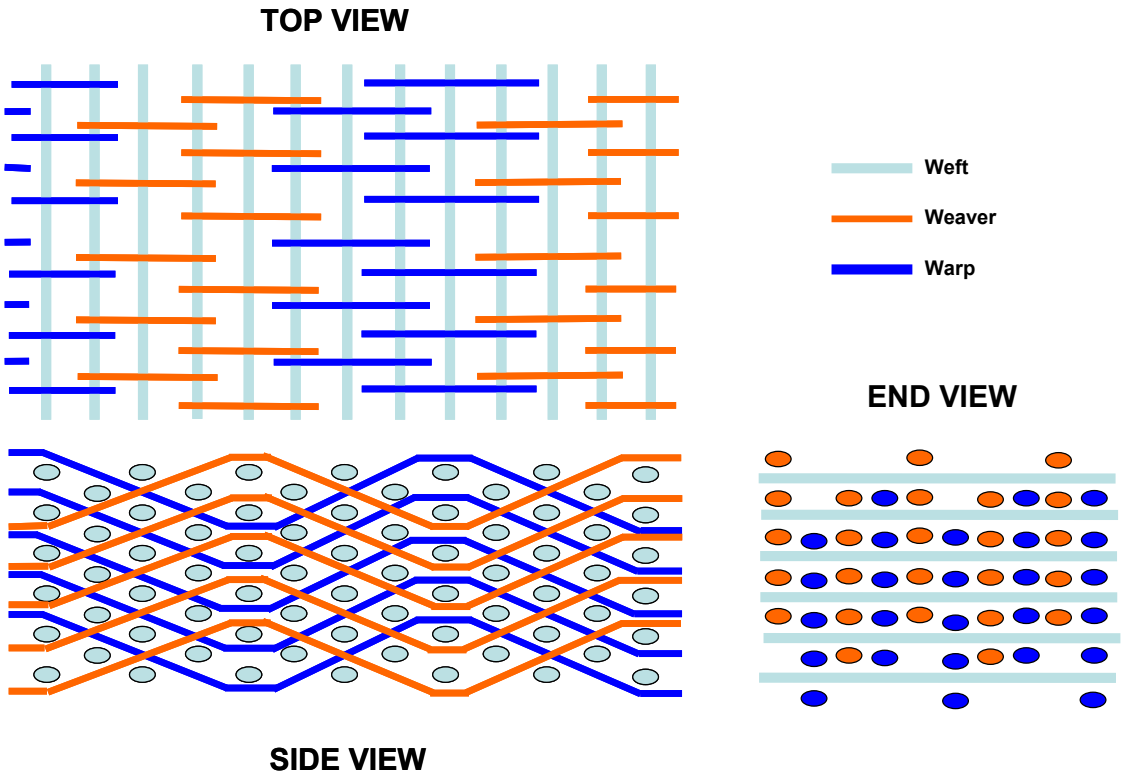

Figure 1 Schematics showing the weave architecture of Fabric A and Fabric B

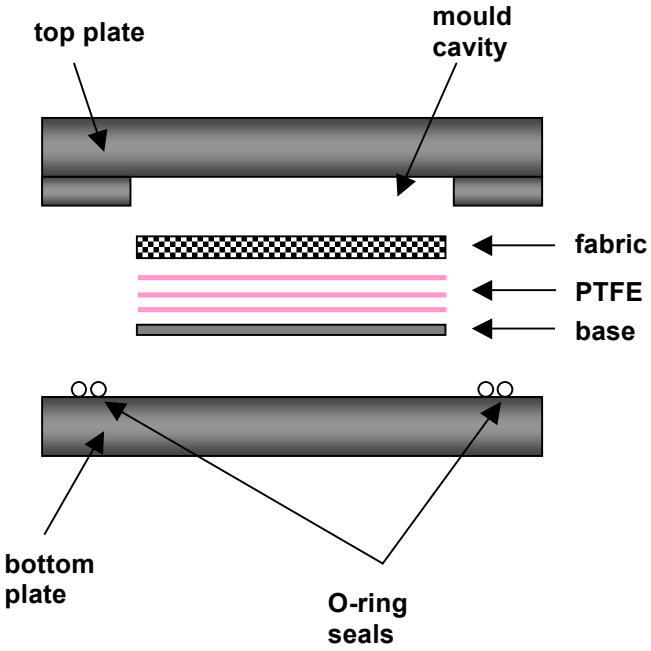

Figure 2: Diagram of RTM mould showing shim plate and fabric configuration

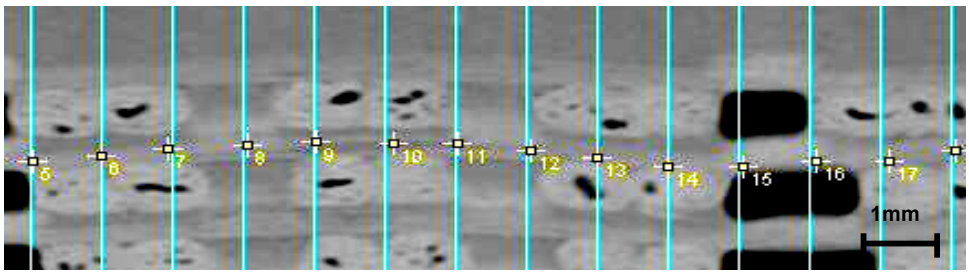

Figure 3: Discretization of the yarn centreline

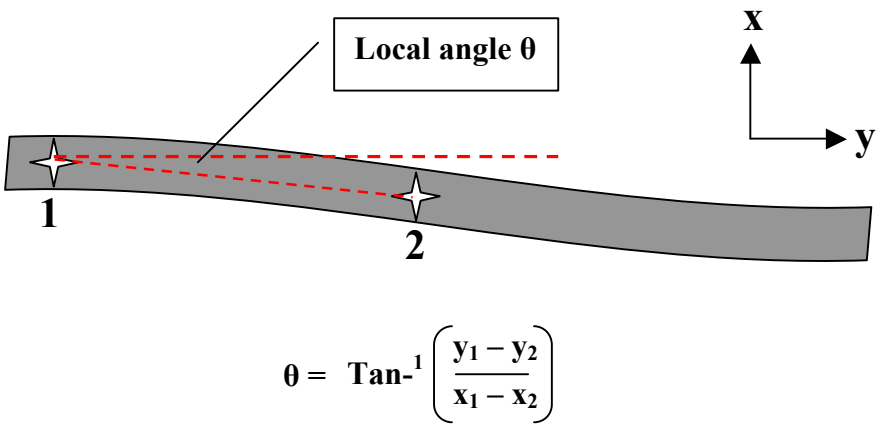

Figure 4: Calculation of the local angle from two points on the yarn centreline

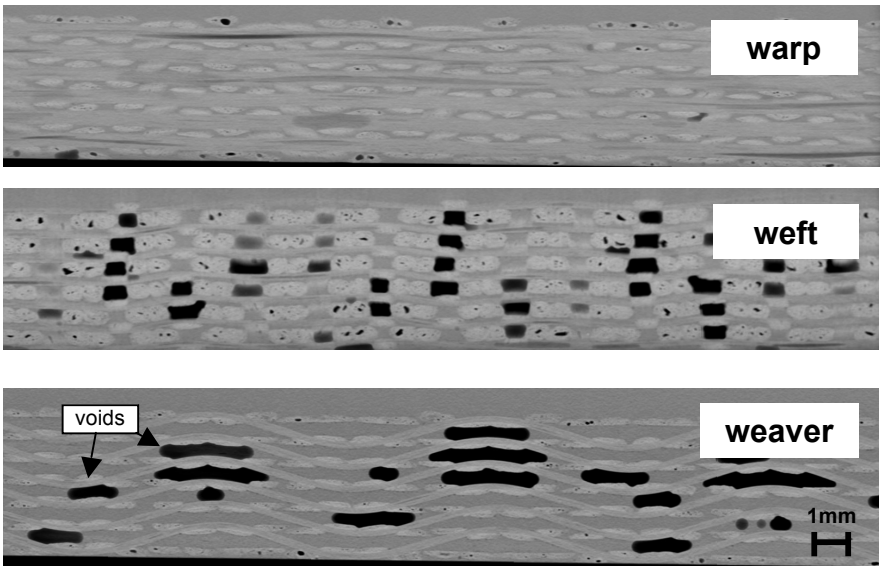

Figure 5: CT scan slices showing yarn profile in Fabric A in as-woven potted samples

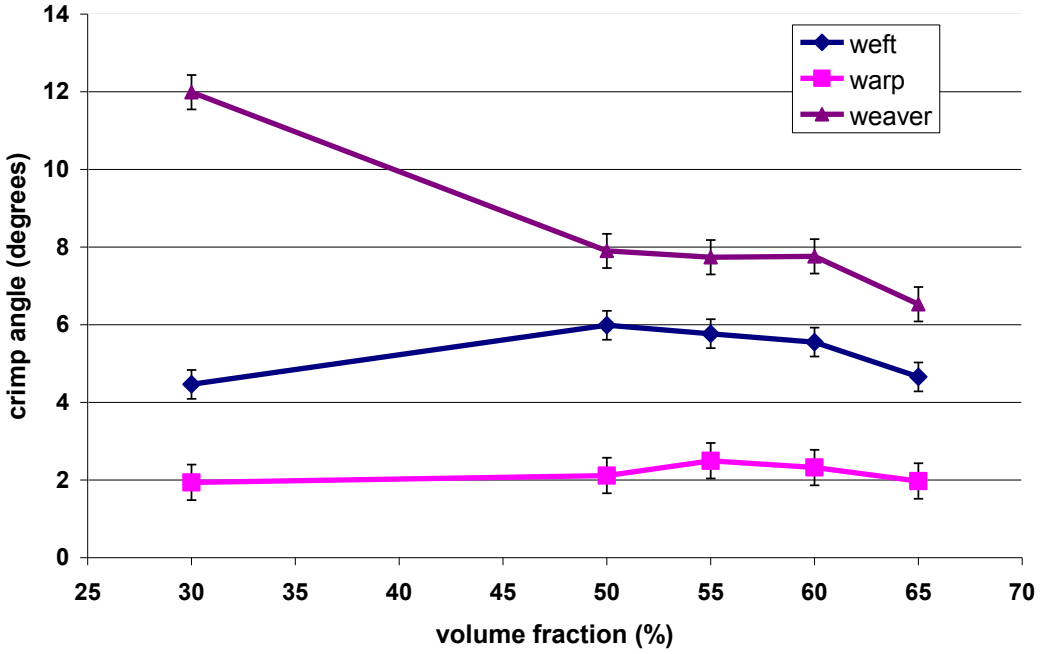

Figure 6: Overall mean yarn crimp for Fabric A

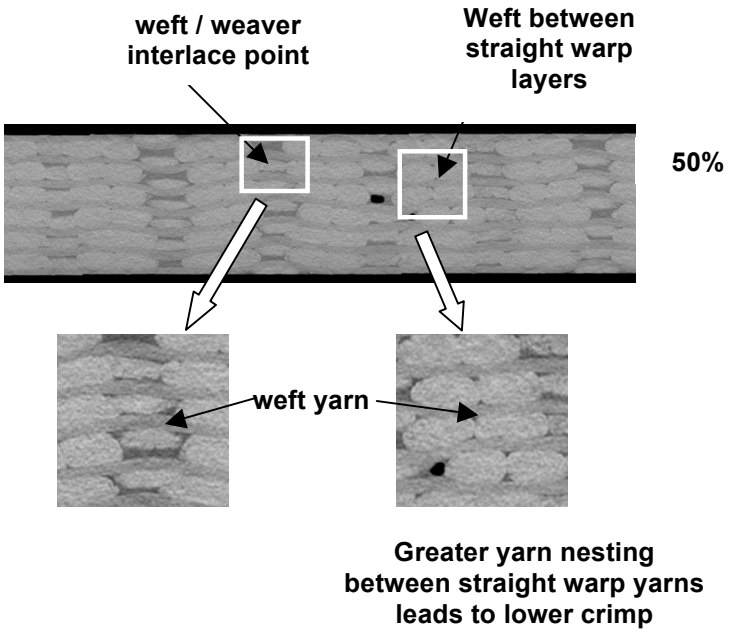

Figure 7: Weft yarn architectural features at 50% volume fraction of Fabric A

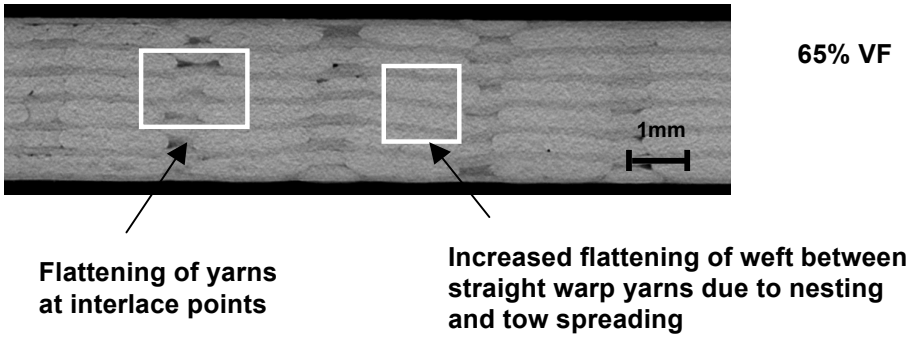

Figure 8: Weft yarn architectural features at 65% volume fraction

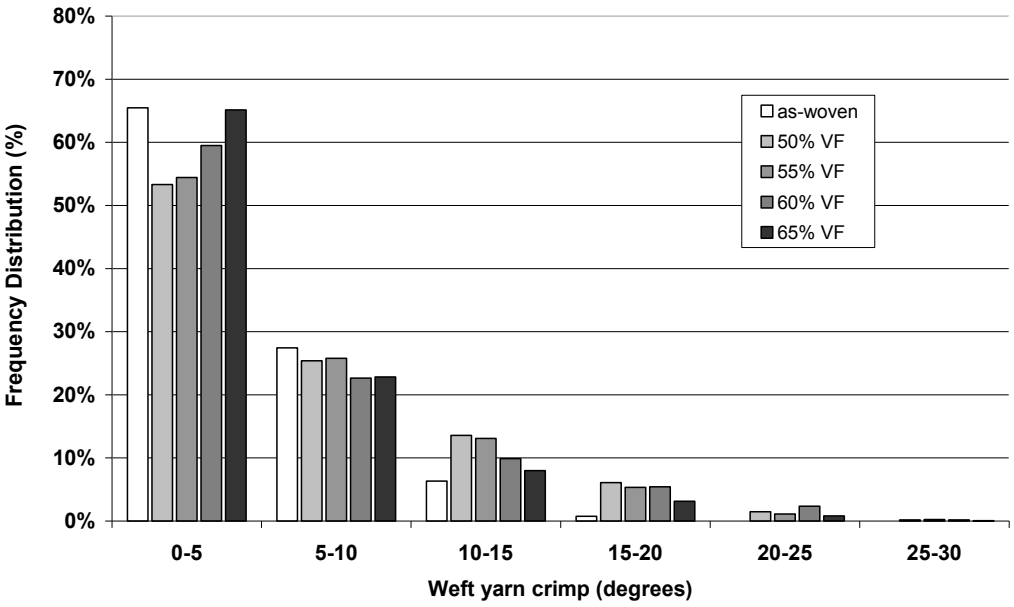

Figure 9: Frequency distribution of weft yarn crimp in Fabric A

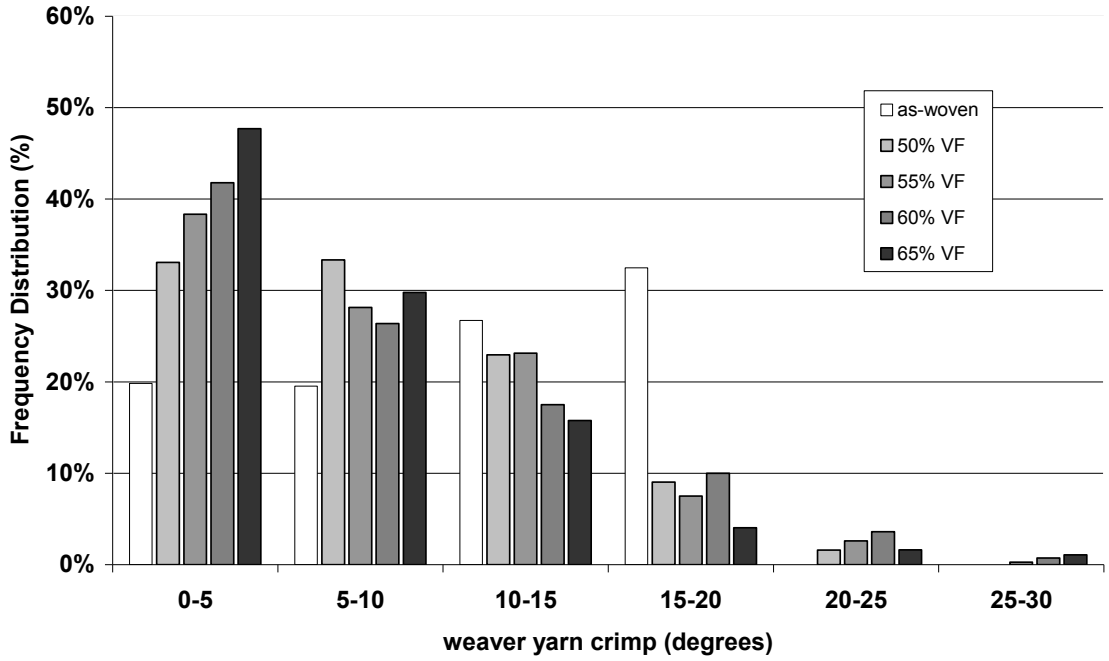

Figure 10: Frequency distribution of weaver yarn crimp in Fabric A

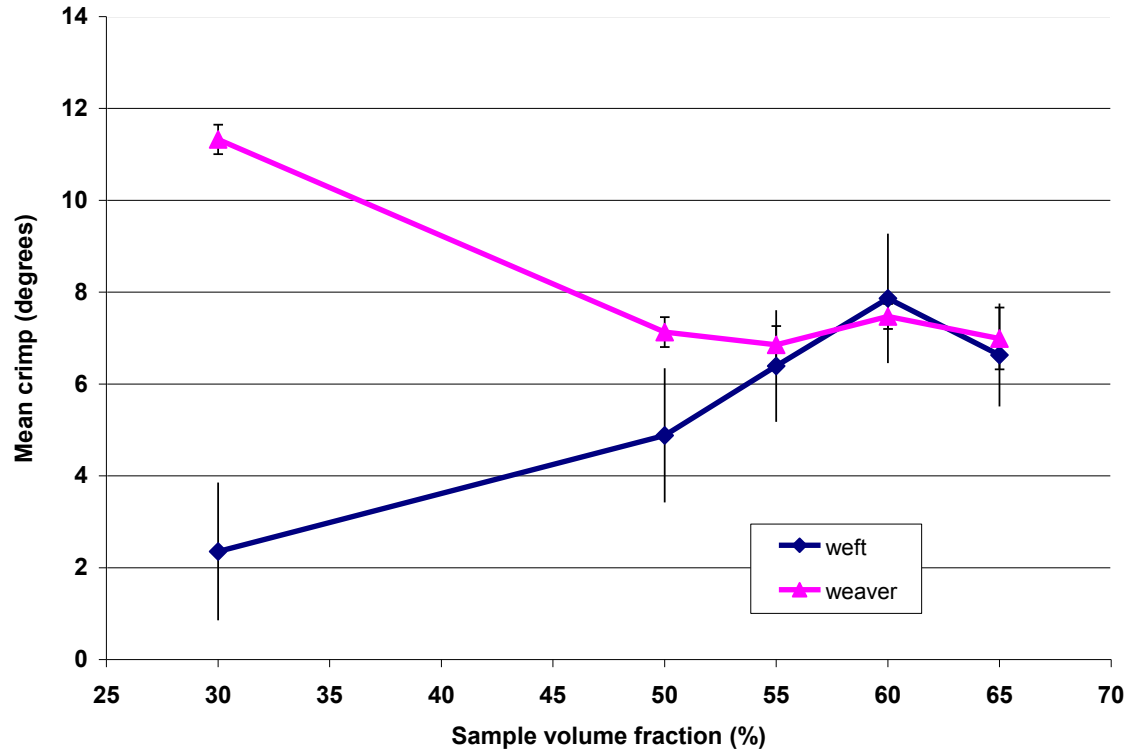

Figure 11: Mean yarn crimp in Fabric B

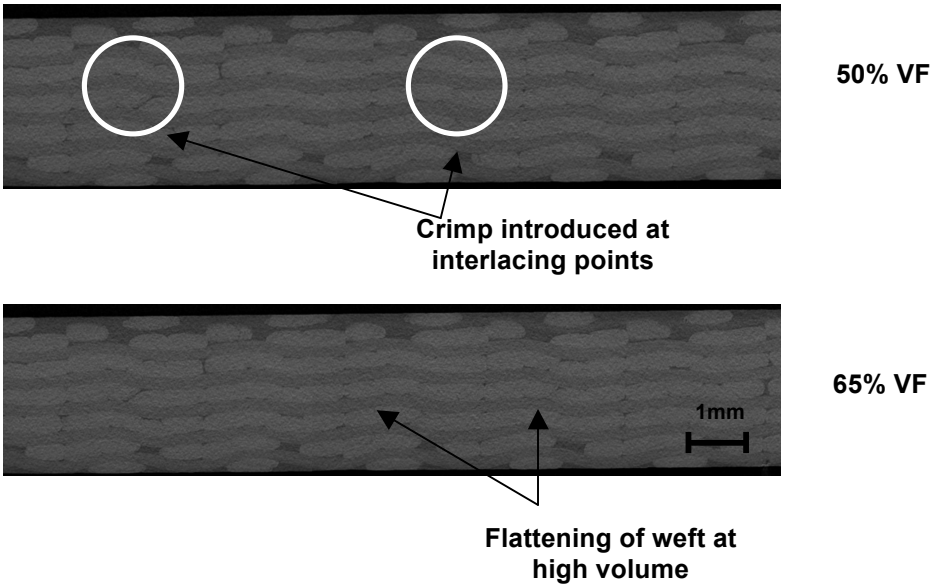

Figure 12: Weft yarn architecture of Fabric B at 50% and 65% volume fraction.

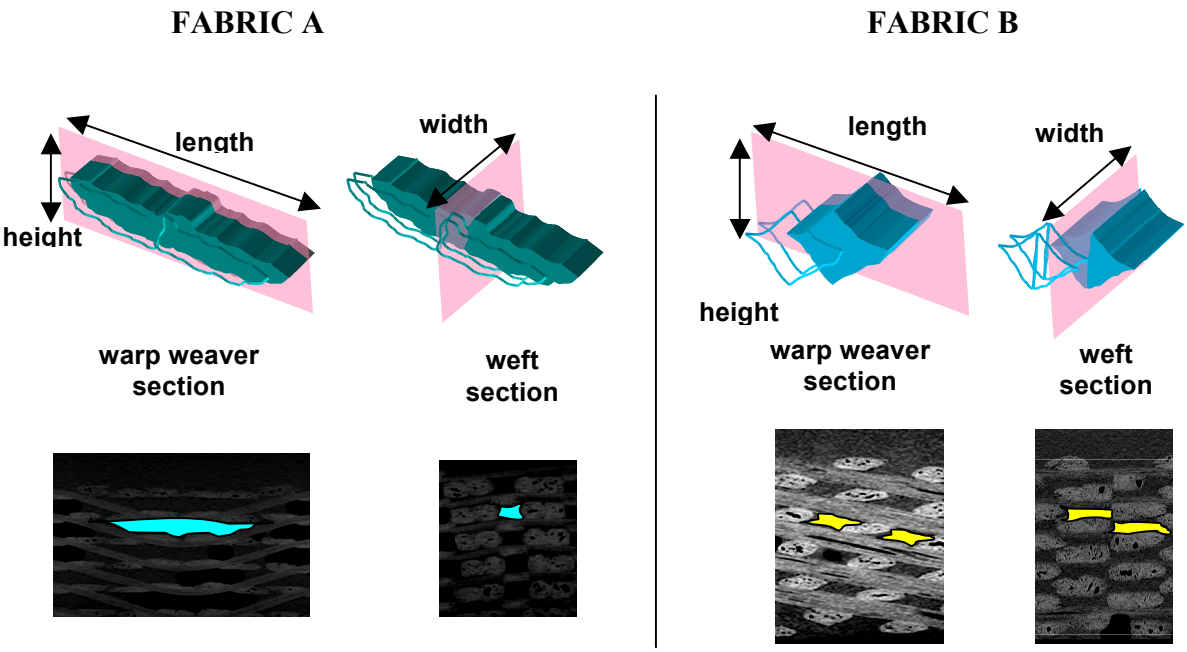

Figure 13: Schematic showing dimension definitions and CT scan views of the weaver resin channel

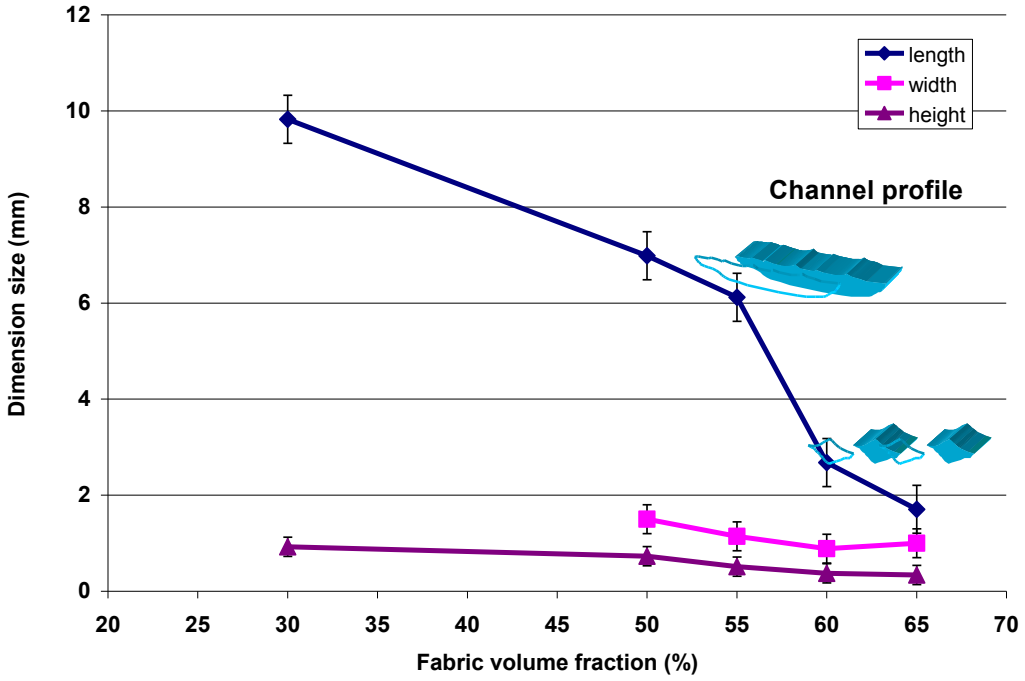

Figure 14: Graph showing resin pocket dimensions in Fabric A at increasing volume fractions

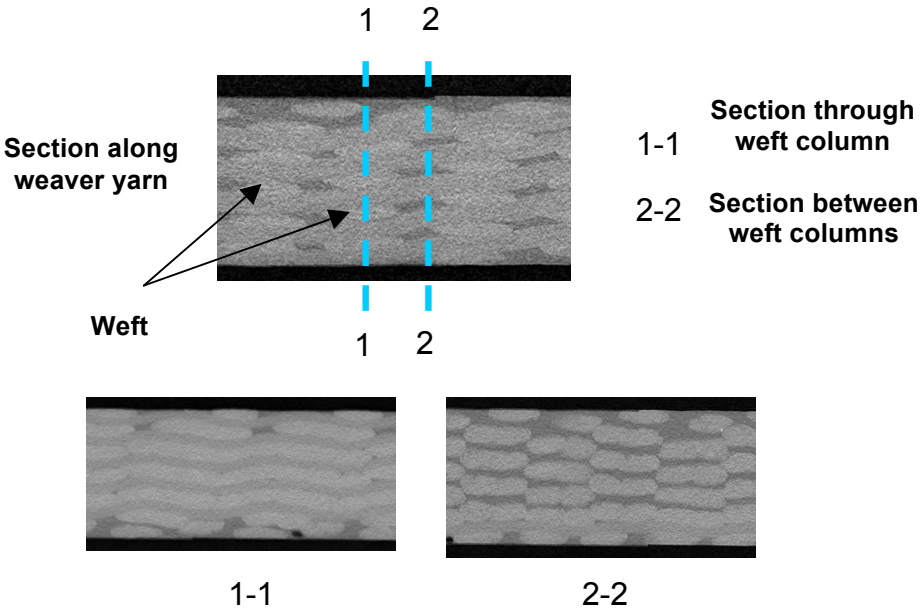

Figure 15: Sections through and between warp layers showing a contrasting presence of resin pockets, Fabric B

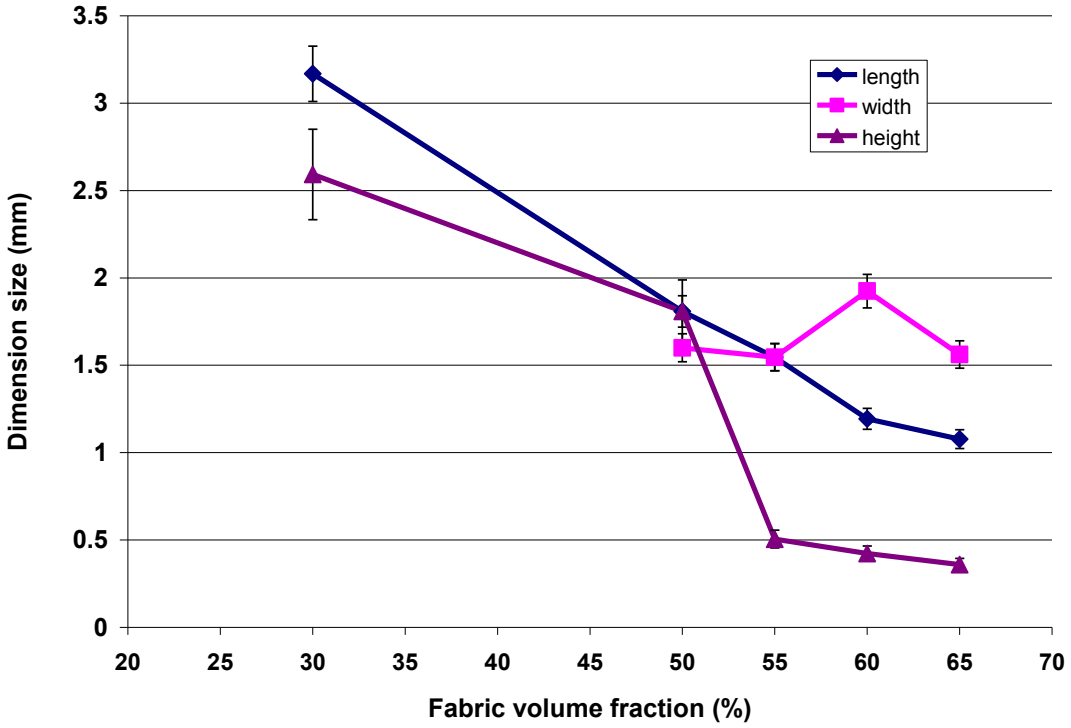

Figure 16: Graph showing resin pocket dimensions in Fabric B